Broadband ferromagnetic resonance of $Ni_{81}Fe_{19}$ wires using a rectifying effect

A. Yamaguchi,[1,2,*] K. Motoi,[1,†] A. Hirohata,[3] H. Miyajima,[1,‡] Y. Miyashita,[1] and Y. Sanada[4]
[1]*Department of Physics, Keio University, Hiyoshi, Yokohama 223-8522, Japan*
[2]*PRESTO, JST, 4-1-8 Honcho Kawaguchi, Saitama 332-0012, Japan*
[3]*Department of Electronics, University of York, Heslington, York YO10 5DD, England*
[4]*Department of Electronics and Electrical Engineering, Keio University, Hiyoshi, Yokohama 223-8522, Japan*
(Received 10 January 2008; revised manuscript received 2 July 2008; published 2 September 2008)

The broadband ferromagnetic resonance (FMR) measurement has been carried out by using a rectifying effect in two sets of $Ni_{81}Fe_{19}$ wires. One wire is deposited on the middle strip line of the coplanar waveguide (CPW) and another is deposited between two strip lines of the CPW, measuring the FMR induced by in-plane and out-of-plane magnetic fields, respectively. The FMR frequency is defined by detecting the magnetoresistance oscillation due to the magnetization dynamics induced by a radio frequency (rf) field. The magnetic-field dependence of the resonance frequency and the rectification spectrum are analytically interpreted based on our uniform magnetization precession model. These findings reveal that two distinct rectifying signals are anticipated by a rf field and a rf current, which can easily be controlled by engineering the ferromagnetic wire shape and the external field orientation. These fundamental understandings are crucial for future rf device applications in spintronics.

DOI: 10.1103/PhysRevB.78.104401 PACS number(s): 76.50.+g, 74.25.Ha, 75.75.+a

I. INTRODUCTION

Magnetization dynamics of nanoscale and micronscale ferromagnets in the radio frequency (rf) and microwave frequency regions is of critical importance to fundamental studies in spintronics. In particular, the ferromagnetic dynamics in the gigahertz region has been actively explored for the applications in microwave devices by using various techniques, such as ferromagnetic resonance (FMR),[1–5] Brillouin light scattering (BLS),[5–8] and time-resolved magneto-optical Kerr effect.[9,10] Each technique, however, has its own advantages and disadvantages for the characterization of the magnetization dynamics in the high-frequency region. In particular, there are two complementary types of experiments, BLS and FMR. The BLS corresponds to scattering photons from thermally excited spin waves traveling with a wave vector and an energy. In this scattering process, the spin wave of the wave vector can be created or annihilated due to the conservation of an energy and a momentum. In contrast, the FMR measurement systems and analytical methods are widely used as compared to the BLS. The FMR excitations transfer no momentum and generate only modes with the total momentum satisfying zero, i.e., uniform modes. In addition, standing spin waves with finite wave vectors are visible in the FMR for reducing sample sizes, where the exchange and magnetostatic energies become important, and are evident pinning conditions at the sample boundaries. When the FMR measurement is carried out on a single small sample, magnetization dynamics with spin waves can be easily obtained. It is therefore crucial to develop a method to analyze the magnetization dynamics properties not only for basic scientific knowledge but also for technical applications.

Recently, several electrical measurements[11–19] have been proposed, which are extremely sensitive and suitable for investigating the magnetization dynamics in submicron-scale magnets. One of them is a pulse-inductive method,[13] which can measure the time domain of dynamical properties in an individual ferromagnetic film and a multilayered spin-valve stack. This method is especially useful for the characterization of intrinsic dynamical properties with recourse to a state-of-the-art storage oscilloscope for high-speed sampling and a wideband amplifier. Besides, a broadband spectrometer is preferable for the FMR studies under a constant magnetic field. The inductive technique to measure the FMR, using a vector network analyzer, provides an insight to a modal spectrum with respect to both frequency and effective damping in the various modes.[11,12]

Currently, intensive investigation on a spin-polarized current has been performed for potential applications to spintronic devices. The spin-polarized current flowing through a ferromagnet generates spin-wave excitation[20,21] together with magnetization reversal, which is a consequence of spin-angular-momentum transfer from the spin-polarized current onto a ferromagnetic moment. One of the most interesting properties is the rectification of a rf current as have reported by Tulapurkar *et al.*[14] in a magnetic tunnel junction and Sakey *et al.*[15] in a spin valve. Such rectification also occurs in thin ferromagnetic films and wires, and was investigated by Juretscheke *et al.*,[16] Yamaguchi *et al.*,[17] Costache *et al.*,[18] and Mecking *et al.*[19] For these structures except for our previous investigation,[17] a direct current (dc) voltage is generated because the rf current flows through the ferromagnets due to the multiplication of the rf current and the magnetoresistance oscillation, which are induced by spin precession by the spin transfer torque and the rf driving field, respectively. Such dc voltage generation by a rf current flowing through a ferromagnet is called a rectifying effect or rectification of a rf current.

In our previous papers,[17] to the contrary, we have demonstrated the rectifying effect induced by the direct injection of a rf current in a submicron ferromagnetic wire. Even so, the physical origins of the driving terms have not been revealed since most of the injected rf current flow through the ferromagnetic strip only to generate a small driving field. In this paper, therefore, we compare the rectifying effect induced by

the direct current injection with that generated by the rf driving field in two distinct geometries and propose a phenomenological model to explain the results obtained from carefully designed ferromagnetic wires. To clarify the physical origin of the driving torque, in particular, we focus on the in-phase magnetization dynamics induced by the rf driving field and the rf current. In Sec. II, sample fabrication and analysis on a conventional magnetic-field mode are described. In Sec. III, a mode for the spin dynamics in a ferromagnetic wire is proposed under the excitation of both in-plane and out-of-plane rf driving fields. In particular, we focus on both a spectrum shape and angle dependence of the rectification due to the in-phase spin dynamics excited by the rf current. Experimental results are shown and compared with our dynamical analytical model in Sec. IV. In Sec. V, we further discuss our experimental results and the validity of our phenomenological analytical approach by comparing our findings with those by the other groups. Finally, conclusions from our investigation are summarized in Sec. VI.

II. SAMPLE FABRICATION AND ANALYSIS ON A MAGNETIC-FIELD MODE

At an equilibrium state, a magnetization maintains its orientation by a local effective field $\boldsymbol{H}_{\mathrm{eff}}$, while the precession of the magnetization is introduced around the equilibrium orientation by the application of a weak microwave pumping field $\boldsymbol{h}_{\mathrm{rf}}$ in a FMR state. This pumping field exerts a small perturbative torque $\boldsymbol{M}\times\boldsymbol{h}_{\mathrm{rf}}$ onto the magnetization and, in consequence, the local effective field exerts a restoring torque $\boldsymbol{M}\times\boldsymbol{H}_{\mathrm{eff}}$. Therefore, when both in-plane and out-of-plane rf fields are applied, two different sets of magnetization dynamics occur with respect to the direction of the applied torque. In order to understand the rectifying effect of the FMR in ferromagnetic $Ni_{81}Fe_{19}$ (Py) wires, we investigate the spin dynamics individually for the in-plane and out-of-plane rf fields by fabricating two types of the wire samples.

By using electron-beam lithography and lift-off processing (see Fig. 1), two kinds of Py wires with thickness of 22 and 30 nm are prepared on MgO (100) substrates; the former is prepared on the top of the coplanar waveguide (CPW) comprising a Cr (5 nm)/Au (38 nm) conductive strip [Fig. 1(a)], while the latter is prepared in the aperture between the conductive strip lines of the CPW, comprising Cr (5 nm)/Au (80 nm) [Fig. 1(b)]. The wire prepared on the CPW strip lines (3 μm wide) is 2 μm in width and 80 μm in length as shown in Fig. 1(a), while the wire prepared between the CPW strip lines (5 μm wide) is 2 μm in width and 150 μm in length as shown in Fig. 1(b).

The ground-signal-ground (GSG)-type microwave probe is connected to the CPW, and the dc voltage difference induced by the rf current flowing through the system is detected by a bias-tee circuit and a voltmeter as illustrated in Fig. 1(c).[17] The sinusoidal voltage output of the signal generator (SG) with a frequency range from 10 MHz to 15 GHz produces an approximately elliptical field pattern h_{RF} around the middle strip line.[22,23] For the arrangement shown in Fig. 1(a), the rf current flowing through the middle strip gives rise to the transverse rf field, while for that shown in Fig. 1(b),

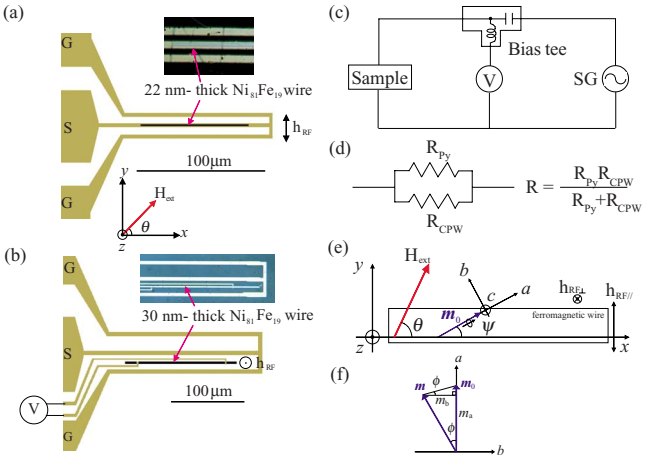

FIG. 1. (Color online) Schematic diagrams and optical microscope images of the devices for the applications of (a) in-plane and (b) out-of-plane magnetic fields. The external static magnetic field (H_{ext}) is applied in the substrate plane at the angle of θ from the longitudinal axis of the wire. Schematic diagrams of (c) the electrical measurement circuit and (d) the equivalent circuit for the device are also illustrated. (e) Schematic projection of the magnetic-moment precession in the *a*-*b* plane.

the rf current across the CPW introduces the rf field perpendicular to the same plane. The external static magnetic field $\boldsymbol{H}_{\mathrm{ext}}$ is additionally applied in the substrate plane as a function of tilting angle θ from the longitudinal axis of the wire. All these FMR measurements are performed at room temperature.

Figures 2(a) and 2(b) show the rf field distributions evaluated by the high-frequency structure simulator (HFSS) (Ref. 24) for the two cases corresponding to Figs. 1(a) and 1(b), respectively. The geometries and dimensions for the simulations are the same as those of the present device structures measured. The calculated rf field distributions, visually shown in Figs. 2(a) and 2(b), are therefore consistent with those in real space.

As shown in Fig. 2(a), the in-plane Oersted field along the y direction, which is produced by the rf current I flowing at a distance z along the z axis, is defined as $H_y(I,z)$ for the device configuration shown in Fig. 1(a), where the y axis is transverse to the current direction. At a position in the vicinity of the center of the Py wire on the middle CPW (width w), the middle wire can be treated as an infinite sheet of a current, which produces a field $h_{\mathrm{in\ plane}}=I/2w$.[13] Similarly, for the device arrangement shown in Fig. 1(b), the out-of-plane field $H_z(I,y)=h_{\mathrm{out\ of\ plane}}=I/2y$ is generated along the wire axis [Fig. 2(b)], where y is the distance between the center of the wire and that of the CPW middle strip line.

III. ANALYTICAL MODEL FOR THE MAGNETIZATION DYNAMICS

The dynamics of a magnetization under a rf field is analytically described by the Landau-Lifshits-Gilbert (LLG) equation. The LLG equation in the coordinate system as shown in Fig. 1(e) is expressed by

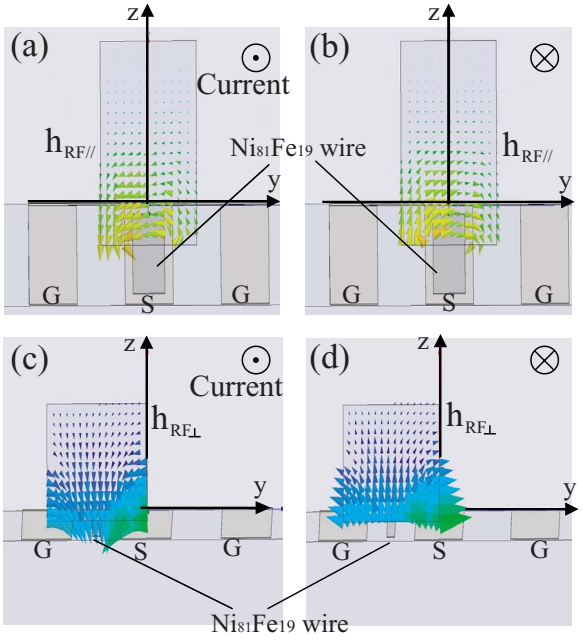

FIG. 2. (Color online) Calculated rf magnetic-field distributions on the Py wire on the middle conductive strip line of the CPW, corresponding to the device in Fig. 1(a), at the phases of (a) 0° and (b) 180°. Those on the Py wire between the middle strip line and one of the ground lines of the CPW [see Fig. 1(b)] at the phase of (c) 0° and (d) 180°. These phases of 0° and 180° correspond to the directions of the current, i.e., $+x$ and $-x$ directions.

$$\frac{\partial \boldsymbol{m}(t)}{\partial t} = -\gamma_0 \boldsymbol{m}(t) \times (\boldsymbol{H}_{\text{eff}} + \boldsymbol{h}_{\text{RF}}) + \alpha \boldsymbol{m}(t) \times \frac{\partial \boldsymbol{m}(t)}{\partial t}, \quad (1)$$

where $\boldsymbol{m}(t)$ denotes the unit vector along the local magnetization ($\boldsymbol{m}=\boldsymbol{M}/M_S$, $|\boldsymbol{m}|=1$, and M_S as the saturation magnetization), and γ_0, $\boldsymbol{H}_{\text{eff}}$, $\boldsymbol{h}_{\text{RF}}$, and α represent a gyromagnetic ratio, an effective magnetic field including exchange and demagnetizing fields, a rf field produced by a rf current flowing through the middle strip of the CPW, and the Gilbert damping constant, respectively.

As schematically shown in Fig. 1(e), we define the (x,y,z) coordinate system, in which three components correspond to the vertical wire axis, the longitudinal wire axis, and the normal to the substrate plane, respectively. The external magnetic field is directed at angle θ from the $+x$-coordinate axis. Subsequently, we also define the (a,b,c) coordinate system, where the $+a$ direction corresponds to the equilibrium direction of $\boldsymbol{m}_0$ along the effective magnetic field $\boldsymbol{H}_{\text{eff}}=\boldsymbol{H}_{\text{ext}}+\boldsymbol{H}_A$ ($\boldsymbol{H}_{\text{ext}}$ as an external field and $\boldsymbol{H}_A$ as a shape anisotropy field). To simplify the analysis and perceive the essence of the phenomena, the uniform macrospin precession in the phase with the rf current is assumed to be dominant in our system because of the strong shape anisotropy.

The magnetization precession around $\boldsymbol{H}_{\text{eff}}$ results in a small time-dependent component of the magnetization perpendicular to $\boldsymbol{m}_0$, which inclines at the angle ψ from the $+x$ axis. Subsequently, we decompose the unit vector $\boldsymbol{m}(t)$ as

$$\boldsymbol{m}(t) = [m_a(t), m_b(t), m_c(t)], \quad (2)$$

where $|\boldsymbol{m}(t)|=1$, and hence, $m_a=\sqrt{1-(m_b^2+m_c^2)}$. The magnetic fields, $\boldsymbol{H}_{\text{eff}}$, $\boldsymbol{H}_{\text{ext}}$, and $\boldsymbol{H}_A$, in the (a,b,c) coordinate system satisfy the following relationship:

$$\boldsymbol{H}_{\text{eff}} = \boldsymbol{H}_{\text{ext}} + \boldsymbol{H}_A. \quad (3)$$

Here,

$$\boldsymbol{H}_{\text{ext}} = [H_{\text{ext}} \cos(\theta-\psi), H_{\text{ext}} \sin(\theta-\psi), 0], \quad (4)$$

and

$$\boldsymbol{H}_A = -M_S \tilde{\boldsymbol{N}} \cdot \boldsymbol{m}, \quad (5)$$

where $\tilde{\boldsymbol{N}}$ is the demagnetizing factor tensor in the (a,b,c) coordinate system, which is given by

$$\tilde{\boldsymbol{N}} = \begin{pmatrix} N_x \cos^2\psi + N_y \sin^2\psi & (N_x - N_y)\cos\psi \sin\psi & 0 \\ (N_x - N_y)\cos\psi \sin\psi & N_x \sin^2\psi + N_y \cos^2\psi & 0 \\ 0 & 0 & N_z \end{pmatrix}, \quad (6)$$

where N_x, N_y, and N_z are the demagnetizing factors in the (x,y,z) system. Equation (6) satisfies the Schlomann sum rule;[25] $\text{Tr}\,\tilde{\boldsymbol{N}}=1$.

In the case of the wire prepared on the conductor strip line [see Fig. 1(a)], the rf field in the plane $\boldsymbol{h}_{\text{RF}\parallel}$ is given by

$$\boldsymbol{h}_{\text{rf}\parallel} = (h_{\text{in plane}} e^{i\omega t} \sin\psi, h_{\text{in plane}} e^{i\omega t} \cos\psi, 0), \quad (7)$$

while for the wires located between the strip lines [see Fig. 1(b)], the rf field perpendicular to the plane $\boldsymbol{h}_{\text{RF}\perp}$ is written by

$$\boldsymbol{h}_{\text{rf}\perp} = (0, 0, h_{\text{out of plane}} e^{i\omega t}). \quad (8)$$

Hereafter, N_x along the wire axis is assumed to be almost zero ($N_x \approx 0$) because the long wire is considered in this study and the easy axis is directed along the x direction, and hence the precession angle around the direction of the effective magnetic field $\boldsymbol{H}_{\text{eff}}$ is assumed to be very small ($m_a \approx 1$ and $dm_a/dt \approx 0$). Accordingly, the small perturbation of the magnetization in the (a,b,c) coordinate system is approximately given by

$$\delta\boldsymbol{m} \approx [0, m_b(t), m_c(t)] \approx (0, m_b e^{i\omega t}, m_c e^{i\omega t}), \quad (9)$$

where ω is the rf angular frequency of the driving fields, $\boldsymbol{h}_{\text{rf}\parallel}$ and $\boldsymbol{h}_{\text{rf}\perp}$. Next, we linearize the LLG equation [Eq. (1)] and reduce to a partial differential equation with respect to the dynamic magnetization components $m_b e^{i\omega t}$ and $m_c e^{i\omega t}$, by taking only the linear terms of m_b and m_c into account. We consider the following two distinct cases dependent upon the driving fields; $\boldsymbol{h}_{\text{rf}\parallel}$ for the Py wire on the middle CPW [Fig. 1(a)] and $\boldsymbol{h}_{\text{rf}\perp}$ for that between the CPW [Fig. 1(b)].

A. Driving field in the wire plane: $\boldsymbol{h}_{\text{RF}\parallel}$

By substituting Eqs. (3), (7), and (9) into Eq. (1) and also by neglecting minor quadratic terms $h_{\text{in plane}} m_c$ and $h_{\text{in plane}} m_b$ by replacing $\partial/\partial t$ with $i\omega$, we obtain

$$\begin{pmatrix} i\omega & [\gamma_0 H_c' + i\omega\alpha] \\ -[\gamma_0 H_b' + i\omega\alpha] & i\omega \end{pmatrix} \begin{pmatrix} m_b \\ m_c \end{pmatrix} = -\gamma_0 \begin{pmatrix} 0 \\ H_{\text{eff}}' e^{-i\omega t} + h_{\text{in plane}} \cos\psi \end{pmatrix}, \tag{10}$$

where

$$H_b' = H_{\text{ext}} \cos(\theta - \psi) + M_S(N_y - N_x)\cos 2\psi, \tag{11}$$

$$H_c' = H_{\text{ext}} \cos(\theta - \psi) + M_S[N_z - (N_x \cos^2\psi + N_y \sin^2\psi)], \tag{12}$$

and

$$H_{\text{eff}}' = H_{\text{ext}} \sin(\theta - \psi) - \frac{1}{2} M_S(N_x - N_y)\sin 2\psi. \tag{13}$$

Equation (10) can be solved as

$$\begin{pmatrix} m_b \\ m_c \end{pmatrix} = \frac{\gamma_0 (H_{\text{eff}}' e^{-i\omega t} + h_{\text{in plane}} \cos\psi)}{\{\omega_k^2 - (1+\alpha^2)^2\omega^2\} + i\omega\alpha\Delta} \begin{pmatrix} [\gamma_0 H + {}_c' i\omega\alpha] \\ -i\omega \end{pmatrix}, \tag{14}$$

where the FMR frequency ω_k and the linewidth $\alpha\Delta$ are, respectively, given by the following relations:

$$\omega_k^2 = \gamma_0^2 H_c' H_b', \tag{15}$$

$$\Delta = \gamma_0 (H_b' + H_c'). \tag{16}$$

To simplify the analysis and perceive the essence of the magnetization dynamics, we focus on the macrospin (uniform) precession. Essentially, since the shape anisotropy loses its importance at high frequencies, the precessional angle should be given by $\sin\phi(t) \approx \langle\sqrt{m_b^2 + m_c^2}\rangle / |\boldsymbol{m}|$. However, if the shape anisotropy is decreased, the analysis, using the macrospin, cannot explain the dynamics. In our measurement, the shape anisotropy is sufficiently maintained because the resonance frequency ω_k is confirmed to be dependent upon the shape anisotropy.[17,26] The out-of-plane component m_c creates the dynamic demagnetizing field and exerts a torque $\propto \boldsymbol{m} \times \delta\boldsymbol{m}$ on the magnetization, rotating it by angle in the plane. As a result, the in-plane components dominate the magnetization precession. In particular, Fig. 1(f) shows the projection of the magnetic moment in the *a*-*b* plane. Here, we calculate the precession angle of $\phi(t)$ and obtain $m_a \approx 1 - |m_b|^2 \sim 1$ by neglecting minor quadratic term $|m_b|^2$. This assumption is applicable for the case when the out-of-plane component m_c is negligibly small due to the strong magnetic shape anisotropy. Accordingly, m_b induces the anisotropic magnetoresistance (AMR) with a magnetization precession angle of $\phi(t)$, namely,

$$\sin\phi(t) \approx \frac{|\delta\boldsymbol{m}|_b}{|\boldsymbol{m}|} \quad \text{and} \quad \sin 2\phi(t) \approx 2\frac{|\delta\boldsymbol{m}|_b}{|\boldsymbol{m}|}. \tag{17}$$

In the rectification of the rf current in the device, the magnetization dynamics induced by the rf current results in the resistance oscillation and the dc voltage (V_0) generation, originating from the AMR effect in the Py wire.[17] For the device, comprising the Py wire prepared on the CPW [see Fig. 1(a)], the rf current $I(t)$ flows through both the CPW line and the Py wire. Accordingly, the rf current is given by

$$I(t) = I_{\text{CPW}}(t) + I_{\text{Py}}(t), \tag{18}$$

where $I_{\text{CPW}}(t)$ and $I_{\text{Py}}(t)$ are the current flowing though the CPW line and the Py wire, respectively. The total resistance $R(t)$ of the system, consisting of parallel resistances for the Py wire $R_{\text{Py}}(t)$ and the CPW line R_{CPW} as shown in Fig. 1(d), is given by

$$R(t) = \frac{R_{\text{Py}}(t) R_{\text{CPW}}}{R_{\text{Py}}(t) + R_{\text{CPW}}}. \tag{19}$$

Since $R_{\text{Py}}(t)$ is derived from the AMR effect,

$$R_{\text{Py}}(t) = R_0 + \Delta R \cos^2[\psi + \phi(t)], \tag{20}$$

where R_0 is the resistance independent of the time t and angle ψ, and $\Delta R \equiv R_{\parallel} - R_{\perp}$ is the resistance difference between the magnetizations parallel and perpendicular to the current. By considering the fact that ΔR is less than about 2% of R_0 for the $Ni_{81}Fe_{19}$ alloy, we can simplify Eq. (19) to be

$$R(t) \approx \frac{R_{\text{CPW}}}{R_{\text{CPW}} + R_0}\{R_0 + \Delta R \cos^2[\psi + \phi(t)]\}. \tag{21}$$

Consequently, $I_{\text{CPW}}(t)$ and $I_{\text{Py}}(t)$ are calculated by

$$I_{\text{CPW}}(t) = \frac{I(t) R_{\text{Py}}(t)}{R_{\text{CPW}} + R_{\text{Py}}(t)} \approx \frac{I(t) R_{\text{Py}}(t)}{R_{\text{CPW}} + R_0}.$$

$$I_{\text{Py}}(t) = \frac{I(t) R_{\text{CPW}}}{R_{\text{CPW}} + R_{\text{Py}}(t)} \approx \frac{I(t) R_{\text{CPW}}}{R_{\text{CPW}} + R_0} \tag{22}$$

The rf current $I(t) = I\cos\omega t$, which flows through the time-dependent resistance of $R(t)$, yields time-dependent voltage difference $V(t) = I(t)R(t)$ across $R(t)$.

It should be noted that this rectification acts as the homodyne demodulation as previously measured[13] and that the observable spectrum of the induced dc voltage $V_0(\omega)$ is a function of ω, which is equal to the frequency of magnetoresistance, independent of the second harmonic term. After substitution of Eqs. (14), (17), (21), and (22) into $V(t)$, we finally obtain

$$V_0(\omega) \approx A(\omega) \frac{R_0 R_{\text{CPW}}}{(R_0 + R_{\text{CPW}})^2} \frac{\Delta R \cdot I^2}{2w} \left[-\frac{1}{2}\sin 2\psi \cos\psi + 2(1 - 2\cos^2\psi)\cos\psi A(\omega) H_{\text{eff}}' \right], \tag{23}$$

where, by using an approximation of $1 + \alpha^2 \approx 1 (\alpha \sim 0.01$ for Py), $A(\omega)$ is given by

$$A(\omega) \approx \frac{\gamma_0^2 H_c' (\omega_k^2 - \omega^2)}{(\omega_k^2 - \omega^2)^2 + \omega^2\alpha^2\Delta^2}. \tag{24}$$

In the case that $|\boldsymbol{H}_{\text{ext}}| \gg |\boldsymbol{H}_A|$, the magnetization aligns almost parallel to $\boldsymbol{H}_{\text{ext}}$, namely, $\psi \approx \theta$. Then, $V_0(\omega)$ becomes proportional to $\sin 2\theta \cos\theta$. On the other hand, when $|\boldsymbol{H}_{\text{ext}}| \ll |\boldsymbol{H}_A|$, the magnetization directs along the longitudinal wire

axis, i.e., $\psi \approx 0$, and hence $V_0(\omega)$ is almost proportional to $H_{\rm ext} \sin\theta$. Consequently, the field and angle dependences of $V_0(\omega)$ are summarized as the following two cases:

$$\text{(i)} \quad V_0(\omega) \propto \sin 2\theta \cos\theta \quad \text{when} \quad |\boldsymbol{H}_{\rm ext}| \gg |\boldsymbol{H}_A|, \tag{25}$$

$$\text{(ii)} \quad V_0(\omega) \propto H_{\rm ext} \sin\theta \quad \text{when} \quad |\boldsymbol{H}_{\rm ext}| \ll |\boldsymbol{H}_A|. \tag{26}$$

Here, we consider the influence of the inductive voltage signal (IVS) given by $dm_y/dt = \cos\psi (dm_b/dt)$,[13] which is closely related to the transverse magnetization through the Faraday induction law. In this case, the θ dependence of the IVS is given by $\cos^2\theta$ for $|\boldsymbol{H}_{\rm ext}| \gg |\boldsymbol{H}_A|$ and $\sin\theta$ for $|\boldsymbol{H}_{\rm ext}| \ll |\boldsymbol{H}_A|$. The measured θ dependence of $V_0(\omega)$ enables us to determinate whether the IVS contributes the rectifying effect or not as discussed in Sec. IV A. The shape anisotropy is not of fundamental importance, however, the FMR frequency of the rectifying effect is influenced by the shape anisotropy field.

B. Driving field perpendicular to the wire: $h_{\rm rf\perp}$

For the Py wire patterned between the middle strip line and one of the ground strip lines of the CPW, the rf field $\boldsymbol{h}_{\rm rf\perp}$ given by Eq. (8) is introduced perpendicular to the wire plane. Likewise to the previous Sec. III A, after the substitution of Eqs. (3), (8), and (9) into Eq. (1), we obtain the following solution with respect to m_b and m_c by again neglecting the quadratic terms $h_{\text{out of plane}} m_c$ and $h_{\text{out of plane}} m_b$ and by replacing $\partial/\partial t$ with $i\omega$;

$$\begin{pmatrix} m_b \\ m_c \end{pmatrix} \approx \frac{\gamma_0\{(\omega_k^2 - \omega^2) - i\omega\alpha\Delta\}}{(\omega_k^2 - \omega^2)^2 + \omega^2\alpha^2\Delta^2} \times \begin{pmatrix} i\omega h_{\text{out of plane}} + (\gamma_0 H + {}'_c i\omega\alpha) H'_{\rm eff} e^{-i\omega t} \\ (\gamma_0 H'_b + i\omega\alpha) h_z - i\omega H'_{\rm eff} e^{-i\omega t} \end{pmatrix}. \tag{27}$$

The rf current $I(t) = I\cos\omega t$ induced by the injection of a quasi-transverse electric and magnetic (quasi-TEM) microwave flows through the Py wire located between the CPW strips. By substituting Eq. (27) into Eq. (20) by using Eq. (17), we calculate $V(t) = I(t)R(t)$. Similarly to the previous section for $\boldsymbol{h}_{\rm RF\parallel}$, we obtain the frequency spectrum of the induced voltage $V_0(\omega)$;

$$V_0(\omega) \approx B(\omega)\omega^2\alpha\Delta R \frac{I'_{\rm CPW} I'_{\rm Py}}{2y} \times \{-\Delta \sin 2\psi + 2(1 - \cos^2\psi) B(\omega)(\omega_k^2 - \omega^2) \times \{2\Delta\gamma_0 H'_c - (\omega_k^2 - \omega^2)\} H'_{\rm eff}\}, \tag{28}$$

where $I'_{\rm Py}$ and $I'_{\rm CPW}$ are the currents flowing through the Py wire and the middle conductive strip line of the CPW, respectively. Here, $B(\omega)$ is given by

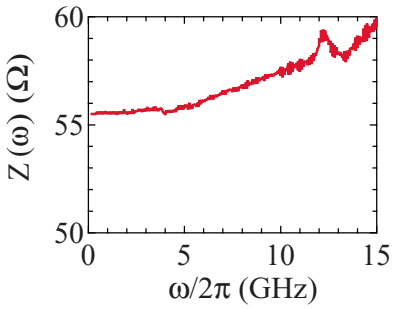

FIG. 3. (Color online) Total impedance of the system $Z(\omega)$ as a function of the rf $\omega/2\pi$ for the Py wire on the middle CPW strip line.

$$B(\omega) \simeq \frac{\gamma_0}{(\omega_k^2 - \omega^2)^2 + \omega^2\alpha^2\Delta^2}. \tag{29}$$

When $|\boldsymbol{H}_{\rm ext}| \gg |\boldsymbol{H}_A|$, the magnetization directs along the applied field ($\psi \approx \theta$) and the rectifying voltage is simply expressed as

$$V_0(\omega) = -B(\omega)\frac{I_{\rm Py} I_{\rm CPW} \Delta R \omega^2 \alpha\Delta}{2y} \sin 2\theta. \tag{30}$$

Therefore, $V_0(\omega)$ becomes proportional to $\sin 2\theta$, which is consistent with the result by Costache *et al.*[18] Conversely, when $|\boldsymbol{H}_{\rm ext}| \ll |\boldsymbol{H}_A|$, the magnetization is almost parallel to the direction of $\boldsymbol{H}_{\rm eff}$, i.e., $0 < \psi(=\text{const}) < \theta$, indicating that $V_0(\omega)$ depends on $\sin\theta$.

IV. EXPERIMENTAL RESULTS OF MAGNETIZATION DYNAMICS

A. Dc voltage induced by the in-plane rf field $h_{\rm rf\parallel}$

In the measured frequency region, the magnetic-field distribution of the CPW agrees very well with that of the quasi-TEM mode[22,23] as seen in Figs. 2(a) and 2(b), showing that the magnetic-field pattern becomes an ellipse around the middle strip conductor. Here, the experimental conditions are as follows: the microwave power injected into the CPW is +5 dBm with $R_{\rm CPW} = 55\ \Omega$ and $R_{\rm Py} = 600\ \Omega$. Due to the impedance mismatching among the measurement cables, the bias tee, the GSG-type microwave probe, and the CPW with the sample, the rf attenuation itself depends on the frequency. In order to evaluate the losses due to this impedance mismatching, we measure the total impedance of the system as a function of the frequency by using a vector network analyzer. For the 2-μm-wide wire prepared on the CPW, the impedance almost monotonically increases with a frequency up to only 10% within the measured frequency as shown in Fig. 3. It is, therefore, safe to address that the total system impedance is almost independent of the frequency within the operational frequency range below 15 GHz. Within this range, the rf current density flowing through the middle coplanar strip line and the Py wire are estimated to be $(6.0-6.2)\times 10^{10}$ and $(7.0-7.2)\times 10^9$ A/m^2, respectively, both values of which are relatively low to induce rf joule heating at the input power of +5 dBm. Accordingly, the am-

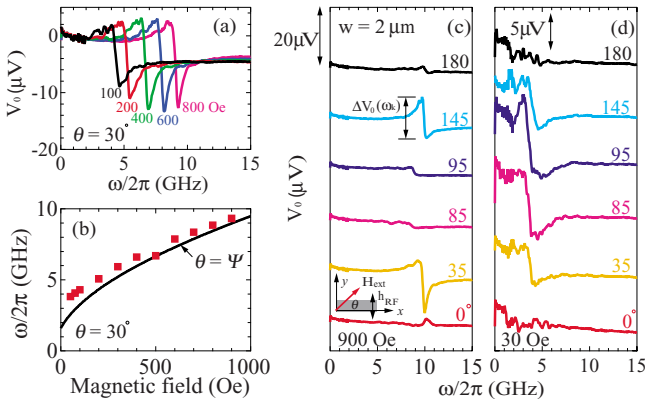

FIG. 4. (Color online) (a) dc voltage spectra $V_0(\omega)$ generated by the 22-nm-thick $Ni_{81}Fe_{19}$ wire on the middle CPW strip line in response to the rf current under the magnetic fields of $|\boldsymbol{H}_{ext}|=100$, 200, 400, 600, and 800 Oe at $\theta=30°$. (b) Average frequency between the peak and the dip of the spectra $V_0(\omega)$ is plotted as a function of the applied magnetic field. The line represents a fit with Eq. (15) to the data. Evolution of $V_0(\omega)$ with the angles θ between the longitudinal wire axis and the magnetic-field direction is also shown for (c) $|\boldsymbol{H}_{ext}|=900$ and (d) 30 Oe. Each resonant response is vertically shifted for clarity.

plitude of the rf field on the middle strip line is estimated to be 15 Oe without any power loss.[11–13]

A series of magnetic fields are applied in the substrate plane every 5° from the wire axis. Figure 4(a) shows the field dependence of the dc voltage, $\Delta V_0(\omega)$, at $\theta=30°$ for the 2-μm-wide Py wire prepared on the CPW. As seen in Fig. 4(a), the peak (dip) positions of the resonance spectrum shift towards the higher frequency by increasing the magnetic field. Figure 4(b) shows the average frequency variations between the peak and the dip for the different frequencies of the rf fields. The (red) solid squares indicate the measured points, while the solid line shows the fit with Eq. (15), which is consistent with Kittel's equation.[1] As the rf field induced by the rf current precesses the magnetization in the wire, the AMR resistance also oscillates at the same resonance frequency. This resistance oscillation generates V_0 combined with the rf current.

The rectifying spectra for the magnetic field of 900 Oe in the substrate plane for $\theta=0°$, 35°, 95°, 145°, and 180° are shown in Fig. 4(c). The θ dependence of the spectra indicates that the uniform precession is disturbed by θ and that the sign of V_0 reverses when the sign of the field is reversed (θ to $\theta+180°$). Here, the main resonance frequency ω_k is defined as the average frequency between the peak and the dip in V_0. The experimental data of both ω_k and ΔV_0 are analyzed as a function of θ by using Eqs. (15), (25), and (26) as described in Sec. III A. Figure 5(a) shows the θ dependence of ω_k under $|\boldsymbol{H}_{ext}|=900$ and 30 Oe. The fitting with Eq. (15) almost follows the measured data for $|\boldsymbol{H}_{ext}|=900$ O_e, while the resonance frequency is almost independent of θ for the case of $|\boldsymbol{H}_{ext}|=30$ O_e. This indicates that the magnetization stays almost parallel to the easy axis of the wire under a small static magnetic field. For the case of $|\boldsymbol{H}_{ext}|=900$ O_e, the discrepancy between the experimental and theoretical results in the θ dependence of ω_k is considered to be caused by the inho-

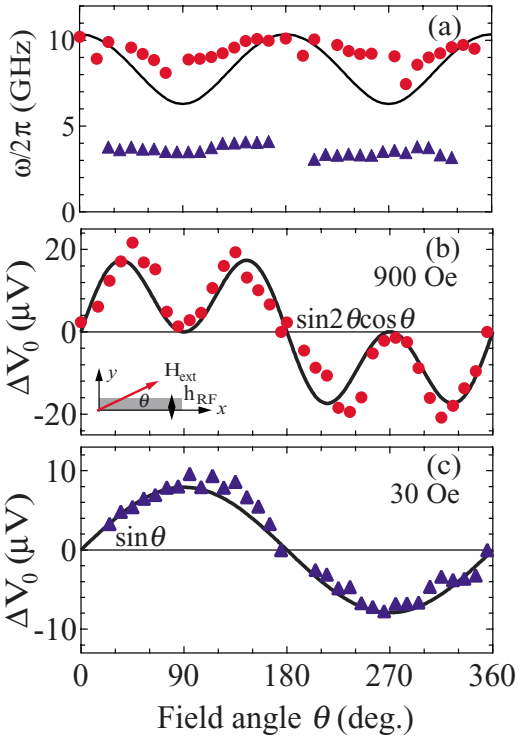

FIG. 5. (Color online) (a) FMR frequency as a function of the applied field angle θ under $|\boldsymbol{H}_{ext}|=900$ (solid circles) and 30 Oe (solid triangles). The (black) solid line represents the corresponding fit with Eq. (15). Under the magnetic fields of (b) $|\boldsymbol{H}_{ext}|=900$ and (c) 30 Oe, the (red) solid circles show the angle θ dependence of the dc voltage difference $\Delta V_0(\omega_k)$ at the FMR frequency. The (black) solid lines represent the corresponding fits with the cases for Eq. (25) and (26).

mogeneity of the magnetization at the edges of the wire.[25,26] The θ dependences of ΔV_0 under $|\boldsymbol{H}_{ext}|=900$ and 30 Oe are shown in Figs. 5(b) and 5(c), respectively. The solid curves represent (a) $\sin 2\theta \cos\theta$ and (b) $\sin\theta$ fits, which are obtained from the calculations for the cases of Eqs. (25) and (26), respectively. As shown in Figs. 5(b) and 5(c), these fitting curves are in good agreement with the experimental results. These experimental results can be explained in terms of the phenomenological analytical model as described in Sec. III A.

To clarify the difference between the mechanism of the rectifying effect induced by the rf driving field and that by the direct rf current injection, we compare the individual spectrum. Figures 6(a) and 6(b) show $V_0(\omega)$ induced by the rf current directly flowing in the 30-nm-thick and 2.2-μm-wide Py wire and by the in-plane rf field for the 22–nm-thick and 2-μm-wide wire attached onto the CPW, respectively. The (red) solid squares show the measured $V_0(\omega)$ data. Reference 17 shows that $V_0(\omega)$ around the FMR frequency ω_k is given by the superposition of a symmetric Lorentzian line shape and an asymmetric dispersion line shape. Conversely, $V_0(\omega)$ is expressed only by the dispersion line shape of Eq. (24), which is due to the disregard of the contribution from the out-of-plane components of the magnetization dynamics. For simplicity, the symmetric (blue line) and asymmetric (pink line) contributions are separately

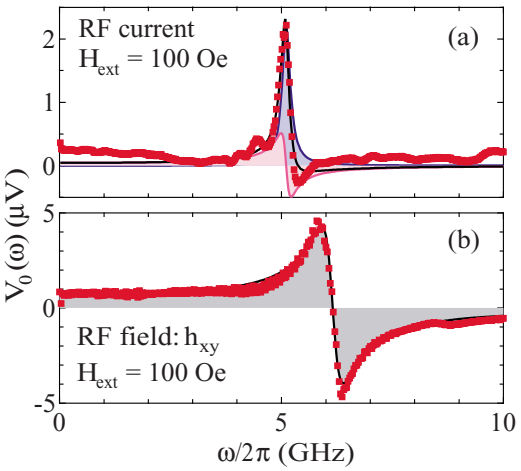

FIG. 6. (Color online) Rectifying spectra $V_0(\omega)$ generated by either (a) the rf current directly flowing through the Py wire or (b) the in-plane rf field. Calculated curves based on our phenomenological analytical model are also shown in both figures.

shown in Fig. 6(a), while only the dispersion contribution (black line) is shown in Fig. 6(b). These fits are in good agreement with the corresponding experimental results.

By comparing the symmetric and asymmetric contributions shown in Fig. 6(a) with those described in Fig. 6(b), we find that the ratio between the symmetric and asymmetric contributions is clearly different. This finding reveals that the magnetization dynamics induced by these two different driving forces is distinctively separated. The candidates of the driving forces for these cases are the spin torque,[20,21] the rf field including the dynamical demagnetizing field,[5,6,28–30] and an inhomogeneous electromagnetic field derived from the coplanar waveguide structure.[23,31] It is natural to consider that the rf field is induced by the rf current,[23,30] while it is necessary to discuss the origin of the spin torque in such a system. The conduction electrons flowing through the ferromagnet with the magnetization distributions may generate both the spin transfer torque[20,21] and the field torque with spatial inhomogeneity.[27,32–34] In particular, the inhomogeneity of the magnetization near the ferromagnet edges,[28–30] where the magnetization is not saturated, creates a complicated domain-wall-like structure and plays an important role on the spin dynamics. According to our previous analysis,[17] the contribution of the spin torque gives the symmetric (absorptive) line shape in coordinate phase with the rf current. On the other hand, the in-plane rf field arises from the out-of-phase magnetization dynamics, yielding the asymmetric (dispersive) line shape induced by the edge magnetization. Here, the demagnetizing field directed normal to the plane by the in-plane rf field forces the magnetization to rotate towards the direction of the effective field. In other words, the symmetric (absorptive) line-shape contribution arises from the rf current in phase with the magnetization dynamics in the FMR state. These understandings and experimental results are principally consistent with those of the Mecking study[19] and are further discussed in Sec. V.

B. Dc voltage induced by the out-of-plane rf field $h_{rf\perp}$

Typical $V_0(\omega)$ spectra for θ=150° under series of H_{ext} are shown in Fig. 7(a). Both the resonance frequency and ΔV_0

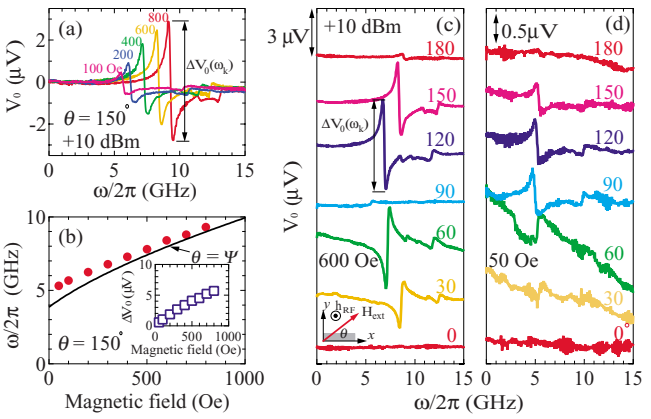

FIG. 7. (Color online) (a) Dc voltage spectra $V_0(\omega)$ generated in the 30-nm-thick Py wire prepared between the middle strip and the ground CPW line in response to the rf current under the magnetic fields of $|\boldsymbol{H}_{ext}|$=100, 200, 400, 600, and 800 Oe at θ=150°. (b) Corresponding average frequency between the peak and the dip of the spectra $V_0(\omega)$ is plotted as a function of the magnetic field. The line shows the fit with Eq. (15) to the data. The inset of (b) represents $\Delta V_0(\omega)$ as a function of the magnetic field. $V_0(\omega)$ for the angles θ between the longitudinal wire axis and the magnetic-field direction is also shown for (c) $|\boldsymbol{H}_{ext}|$=600 and (d) 50 Oe. Each resonant response is vertically shifted for clarity.

increase with increasing the magnetic field. Figures 7(c) and 7(d) show $\Delta V_0(\omega)$ from θ=0°–180° under $|H_{ext}|$=600 and 50 Oe, respectively. As seen in Fig. 7(c) for $|H_{ext}|$=600 O_e, the resonance frequency ω_k shows the minimum at θ=90° and the maxima at θ=0° and θ=180°, while $\Delta V_0(\omega)$ has the minima at θ=0°, 90°, and 180°.

Minor peaks observed at a higher frequency than ω_k in the traces of Figs. 7(a), 7(c), and 7(d) may be the additional spin-wave modes. We note, however, only the dominant mode is employed for the analytical calculations and the data interpretation. Figure 7(b) shows the static field dependence of ω_k. The (red) solid circles are the experimental data, while the black solid line shows the fitting with the analytical equation given by Eq. (15). The almost perfect agreement with the fitting demonstrates that the magnetization vector of the wire is driven into the uniform precession mode. The inset of Fig. 7(b) illustrates the variation of $\Delta V_0(\omega)$ with the magnetic field, where (blue) open squares are the experimental data, illustrating that $\Delta V_0(\omega)$ at the FMR frequency monotonically increases with increasing the magnetic field. According to Eq. (30), $\Delta V_0(\omega)$ at the FMR frequency ω_k is given by

$$\Delta V_0 \propto \omega_k^2 \Delta = \gamma_0^3 M_S H_c' H_b' (H_b' + H_c'). \tag{31}$$

When the demagnetizing field is much larger than the applied field, we obtain $H_c' \approx M_S$ and $\Delta V_0 \propto H_b'$, indicating that the dominant mode is the uniform precessional mode, which is consistent with the model described by Costache *et al.*[18]

Figure 8(a) shows the FMR frequency ω_k under $|H_{ext}|$ =600 and 50 Oe as a function of θ. The results in Fig. 8(a) are almost similar to those in Fig. 5(a), and the fitting agrees in an unambiguous manner with the measured results. As have already mentioned in the previous section, the magne-

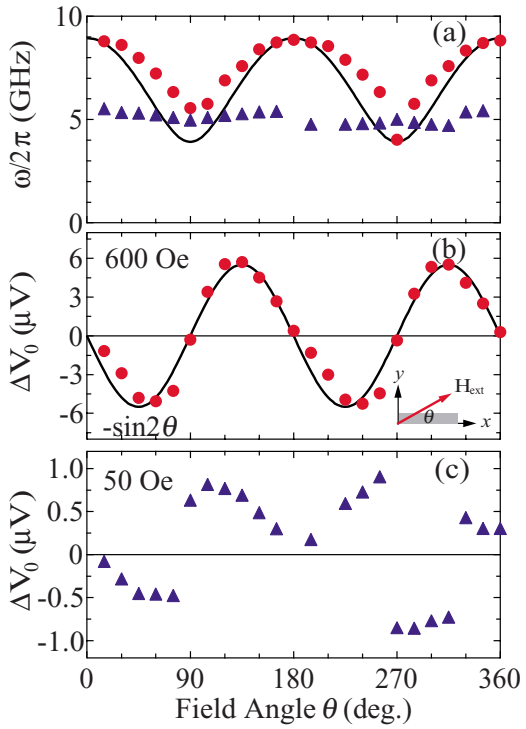

FIG. 8. (Color online) (a) FMR frequency as a function of the applied field angle θ under $|\boldsymbol{H}_{\text{ext}}|=600$ (red solid circles) and 50 Oe (blue solid triangles). The black solid line represents the corresponding fit with Eq. (15). Under the magnetic fields of (b) $|\boldsymbol{H}_{\text{ext}}|=600$ and (c) 50 Oe, the (red) solid circles show the angle θ dependence of the dc voltage difference $\Delta V_0(\omega)$ at the FMR frequency. The black solid line in (b) represents the corresponding fit with Eq. (30).

tization aligns almost along the longitudinal wire axis under a small static applied field, while the magnetization near the edges of the wire is not saturated even when the applied field exceeds its effective anisotropy field $|\boldsymbol{H}_A|$. The θ dependences of ΔV_0 under $|H_{\text{ext}}|=600$ and 50 Oe are also shown in Figs. 8(b) and 8(c), respectively. The (red) solid circles are the experimental data. The (black) solid line in Fig. 8(b) shows a $-\sin 2\theta$ curve, which fits to the data very well. This indicates that the uniform precession mode is dominant under the magnetic fields large enough to direct the magnetization along to the external field. The angle dependence in Fig. 8(c), however, is difficult to explain using solely the uniform precession mode generated by the rf field perpendicular to the plane. The origin of the θ dependence of $\Delta V_0(\omega_k)$ for this case is due to the higher-order spin-wave excitation as observed in shape-controlled ferromagnets.[1–12,15,17,26,28–30]

V. DISCUSSIONS

Before further discussing the rectifying effect of the rf current in our experiment, we provide the detailed comparison of our results with those by the other groups.

Mecking *et al.*[19] have used the TE01 mode using the Ku band (12.4–18 GHz) with the WR62 waveguide and have measured a dc voltage due to the rectification between a rf electric field and time-dependent AMR induced by the rf magnetic field. Their ferromagnetic strip is mounted at the end of the waveguide. This experimental setup allows the rf electric field to be parallel to the Py strip, maintaining the rf magnetic field perpendicular to the Py strip in the film plane. Here, the rf-induced electromagnetic field, which is the origin of the driving torque for the magnetization dynamics, is not fully homogenous at the Py strip due to their device size and arrangement. Even so, the external-field-angle dependence of ΔV_0 is proportional to $\sin 2\theta \cos\theta$ and the spectrum shape is separated into the symmetric and asymmetric contributions, which agrees well with our findings as described in Sec. IV A. However, it should be noted that an inhomogeneous rf driving field does also produce both the symmetric and asymmetric contributions. Therefore, the physical origin of the rectifying effect induced by the direct rf current flowing through a micronscale or nanoscale Py wire remains as an open question to be discussed below.

Costache *et al.*[18] then presented on-chip resonant driving of the uniform magnetization precession mode in a single nanoscale Py strip by the out-of-plane field application. The rectifying signal is derived from the multiple of the induced alternating current (ac) in the strip and the time-dependent AMR. Their analytical model predicts the ΔV_0 is proportional to $\sin 2\theta$, and they have demonstrated partial field angle dependence in their experimental work. Our present work perfectly complement their experimental result for the angle dependence of ΔV_0. In order to reach a consensus on the rectifying effect induced by the rf current, both in-plane and out-of-plane rf fields onto a Py wire need to be independently investigated to evaluate spin dynamics individually for the in-plane and out-of-plane rf fields. We have therefore fabricated two types of the wire samples for these corresponding fields to assess the rectification by the rf current in the Py wire.

Our system presented here is comprised of the ungrounded CPW, which is directly deposited onto the unclad substrate. The ungrounded CPW is a transmission line system consisting of a middle current currying trace with side grounds, extending beyond symmetric gap to both sides of the trace atop of the substrate. The CPW is then connected to the GSG-type microwave probe. The side grounds of the CPW provide the only return current paths. The advantage of using the CPW lies to measure the spin dynamics in a single micronscale or nanoscale magnet because of its high sensitivities. When the quasi-TEM-mode field is directly injected into the conductive line by using the GSG-type microwave probe, the rf electric current only flows through the conductive line. Here, electromagnetic fields are formed symmetrically to the both sides of the middle trace; an electric field $\boldsymbol{E}$ induced by each ground line to the trace and vice versa in phase, and a magnetic field $\boldsymbol{H}$ circulated around the middle trace with the same phase as well. In our configuration, the elecromagneitc field distribution perpendicular to the substrate plane axis depends on the substrate thickness, coplanar waveguide structure, and materials,[23] all of which may additionally induce the rf driving torque. Figure 9 shows the magnetic-field distribution calculated by the HFSS.[24] The device structure for the calculation is the same as the experiment. The vector magnetic-field distribution and the contour diagram of the field magnitude are shown in Figs. 9(a) and

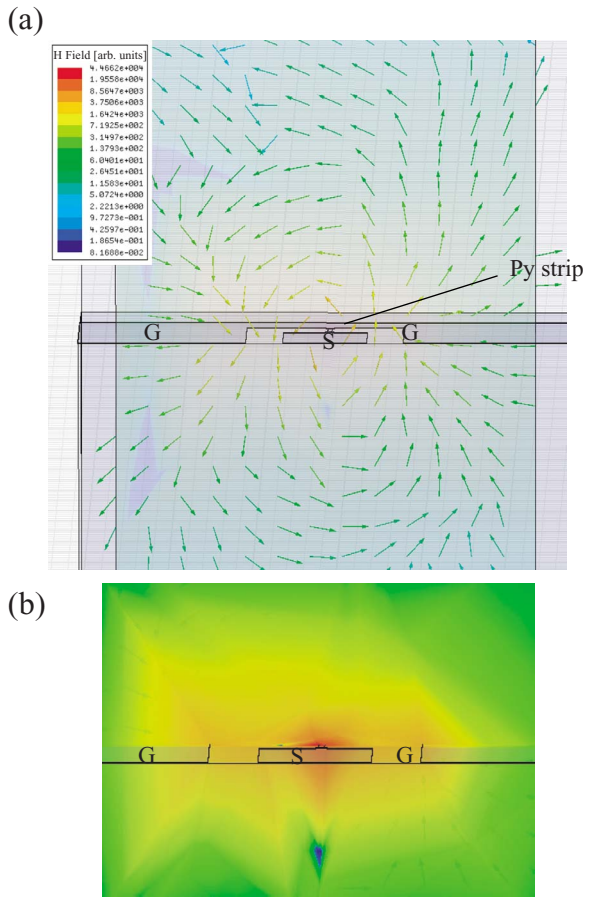

FIG. 9. (Color online) (a) Vector magnetic-field distribution and (b) contour diagram of the field magnitude calculated by HFSS with slant electrodes for clarity.

9(b), respectively. As shown in Fig. 9, the magnetic-field distribution show minor asymmetry at both the top and bottom surfaces of the strip. Such an asymmetric field distribution may additionally induce the rf driving magnetic field. Our systems are short circuited to achieve the one port measurement, which may also provide minor parasitic electromagnetic modes. In our setup, we measure the same rectifying effect in different devices with symmetric transmission lines, confirming the reproducibility of our experiment.

Now, the question we need to answer is how the rf current rectification is generated in the straight Py wire under a uniform magnetization distribution. It is also important to differentiate the rectifying signals excited by the rf current and the rf field, which are coupled with each other according to Maxwell's equations. First, the physical origin of the rectifying effect of the rf current flowing through the straight Py strip is discussed by considering the rf magnetic field, spin torque, and the other nonlinear effects. To understand the rectifying effect, we analytically calculate magnetization dynamics induced by these torques. Our approach derives both the angle dependence of ΔV_0 and the rectifying signals consisting of the different driving torque contributions. Therefore, we demonstrate the detection of the FMR in two distinct systems; a single micronscale Py wire located (i) on the top of the middle trace line and (ii) between the middle and one of the ground traces. The former Py wire experiences predominantly an in-plane rf field, while the latter feels an out-of-plane rf field in principle. The distributions of the both rf-driving fields are designed to be homogeneous at the Py wires. Here, the phase of the rf field is maintained to be the same as that of the injected rf current. The former and the latter device arrangements correspond to the two experimental setups reported by Mecking *et al.*[19] and Costache *et al.*,[18] respectively. By comparing these setups, we analytically distinguish the rf field components in phase with the injected rf current by focusing on the in-phase components only.

We now evaluate the effective rf magnetic field either in-plane or out-of-plane, which consists of an external rf field as well as a rf field induced by the magnetization dynamics and drives the magnetization dynamics inside the Py wire. Here, we assume a uniform magnetization precession to simplify our analytical model to assess these fields. When the direction of the driving field is determined, the precession component is deduced to Eqs. (14) and (27), including the effective field inside the Py wire through the demagnetizing tensor. The effective field consists of a static external field and minor dynamics with both in-plane and out-of-plane contributions when the higher spin-wave modes are excited.[1–6,28–30] If the higher-order spin-wave modes are taken into account for the effective field, the rectifying spectrum is expected to be given by the superposition of the Lorentzian and dispersion-type curves. To clarify the physical origin of the driving torque, we focus on the in-phase magnetization dynamics induced by the rf driving field and the rf current.[35] By assuming that the uniform precession is driven by either the in-plane or out-of-plane rf fields, we describe both the magnetization dynamics and the phenomenological rectifying effect. This leads to the fact that for the in-plane-driving rf field, Eqs. (25) and (26) ideally have only the dispersive term, which is consistent with our experimental results as shown in Fig. 6(b). Conversely, it is clear that the symmetric contribution dominates the spectrum line shape for the case of the direct rf current introduction through the Py wire as shown in Fig. 6(a). This clear distinction is attributed to the differences in the mechanism to induce the rectifying effects by the rf field and the rf current as follows.

We first consider the rectification by the rf current flowing though the Py wire. In our experiment, the rf current in the form of a sinusoidal constant wave is directly injected into the Py wire. The rf current flowing in the loop of the CPW Au electrodes generates an additional Oersted field onto the Py wire, however, the field perpendicular to the substrate plane is canceled out at the wire position because of the symmetrical arrangement of the Au electrode. Even though we confirm that the homogeneous Oersted field induced by the rf current flowing through the Py strip cannot excite the magnetization precession by using micromagnetic simulation,[26] the small inhomogeneous electromagnetic field distribution can induce the magnetization dynamics[23,31] (see Fig. 9), which we have observed experimentally to be the rectifying effect excited only by the rf field as shown in Sec. IV. In addition, the inhomogeneity of the magnetization near the Py wire edges[28,29] and a dynamic dipolar field,[29,30] where the magnetization is not uniform, form complicated domain-wall-like structures and govern the magnetization dynamics.

The conduction electrons flowing through the ferromagnet with the spatial magnetization distribution may also induce the nonlinear torque including the spin transfer torque and the field torque with the spatial inhomogeneity,[27,32–34] generating a similar FMR signal.[35] In fact, we have previously confirmed that a complicated rectifying signal due to the magnetization dynamics is induced by the nonlinear torque in a single domain wall.[17] Paradoxically, spin-wave instability theoretically predicted is introduced by a spin current applied to a uniform ferromagnet, which can also be the origin of the nonlinear torque.[36]

Accordingly, we carefully assess the rectifying effect excited by both the in-plane and out-of-plane rf fields. Since our devices are small enough to match the microwave wavelength, we estimate the in-phase magnetization dynamics with both rf fields and evaluate the difference between the experimental results and our phenomenological analytical model. For our experimental results on the device illustrated in Fig. 1(a), the asymmetric (dispersive) line shape arises from the magnetization dynamics contribution due to the in-plane rf field and the angle θ dependence of ΔV_0 is proportional to $\sin 2\theta \cos\theta$ and $\sin\theta$ for $|\boldsymbol{H}_{\mathrm{ext}}| \gg |\boldsymbol{H}_A|$ and $|\boldsymbol{H}_{\mathrm{ext}}| \leq |\boldsymbol{H}_A|$, respectively (see Fig. 5). These angle dependences are consistent with those induced by the rf current as discussed earlier. On the other hand, the angle θ dependence of ΔV_0 induced by the out-of-plane rf-field excitation is in good agreement with the $\sin 2\theta$ fitting for $|\boldsymbol{H}_{\mathrm{ext}}| > |\boldsymbol{H}_A|$ as shown in Fig. 8. These significant differences between the rf-field orientations clearly indicate that the out-of-plane rf field hardly contributes to the rectifying signal induced by the rf current, of which the field angle dependence is consistent with that of the in-plane rf field excitation. This suggests that the rectification of the rf current in the Py wires may be caused by the in-plane inhomogeneous rf field distribution due to the CPW structure[23,31] (see Fig. 9), which may depart from our analytical model for the ideal case.

As seen in Fig. 6, we find the individual spectrum shape induced by the in-plane rf field and the direct rf current flow is different but with minor spin-wave modes, which means that a dominant direction of the driving torque becomes perpendicular to the Py wire and induces the perpendicular magnetization dynamics.[37] It should be noted that the magnetization dynamics induced by the dynamic field distribution of the higher-order spin-wave modes can also generate an out-of-plane rf driving field contribution both in-phase and out-of-phase. If the in-phase out-of-plane rf driving field contributes to the in-phase magnetization dynamics in the Py wire on the middle strip line [see Fig. 1(a)], the spectrum shape is expected to become a superposition of the symmetric and asymmetric contributions in a FMR state. According to our measurement, however, the line shape shown in Fig. 6(b) holds the asymmetric contribution only. In our systems, the spectrum shape depends only on the in-plane rf field excitation with the homogeneous distribution, which can be explained not by the out-of-phase driving field but by the in-phase field using our phenomenological model as described in Sec. III A. Therefore, we conclude that the asymmetric rectifying spectrum is induced by the homogeneous in-phase in-plane rf driving field, which is uniformly distributed in the Py strip on the middle strip line of the CPW, while the symmetric rectifying spectrum is generated by the in-phase rf current directly flowing through the Py strip.[23,31] Further systematic investigation is necessary in order to perfectly reproduce our analytical model in an ideal sample configuration.

VI. CONCLUSIONS

We have demonstrated the rectifying broadband FMR spectroscopy for micron-scale ferromagnetic wires induced by both the in-plane and out-of-plane components of a uniform rf field by using the CPW method. We successfully explain dc voltage spectra $V_0(\omega)$ measured in the Py wires by our phenomenological and analytical model based on the coupling between the rf current and the AMR oscillation derived from the uniform magnetization precession.

We also find that the characteristic shape of the rectifying spectrum generated by the in-plane rf field differs from that induced by the rf current directly flowing through the Py wire. Similar difference is obtained in the rectifying voltage with respect to the external field orientations, clearly revealing that the phase difference between the rf current and the rf field is 90° by analyzing the in-phase magnetization dynamics induced by the uniform rf driving field.

Such broadband rectifying effect generated by both the in-plane and out-of-plane components of the rf field offers highly sensitive measurement of spin dynamics in nanoscale ferromagnets. The effect can be easily tuned by controlling the resonance frequency by precisely designing either the shape of the Py wire or the magnetic-field applications and hence can facilitate fresh development for future rf spintronics devices.

ACKNOWLEDGMENTS

We thank A. Thiaville and Y. Nakatani for useful discussions. The present work was partly supported by MEXT Grants-in-Aid for Scientific Research in Priority Areas, JSPS Grants-in-Aid for Scientific Research, and the Keio Leading-Edge Laboratory of Science and Technology project 2007.

*Corresponding author: yamaguch@phys.keio.ac.jp
†kmotoi@phys.keio.ac.jp
‡miyajima@phys.keio.ac.jp

[1] C. Kittel, *Introduction to Solid State Physics*, 6th ed. (Wiley, New York, 1986), Chap. 16.
[2] M. H. Seavey, Jr., and P. E. Tannenwald, Phys. Rev. Lett. **1**, 168 (1958).
[3] P. E. Wigen, C. F. Kooi, and M. R. Shanabarger, Phys. Rev. Lett. **9**, 206 (1962).
[4] F. Schreiber and Z. Frait, Phys. Rev. B **54**, 6473 (1996).

[5] *Spin Dynamics in Confined Magnetic Structures*, edited by B. Hillebrands and K. E. Ounadjela (Springer, Berlin, Heidelberg, 2002), Vol. I.
[6] C. Bayer, S. O. Demokritov, B. Hillebrands, and A. N. Slavin, Appl. Phys. Lett. **82**, 607 (2003); C. Bayer, J. Jorzick, B. Hillebrands, S. O. Demokritov, R. Kouba, R. Bozinoski, A. N. Slavin, K. Y. Guslienko, D. V. Berkov, N. L. Gorn, and M. P. Kostylev, Phys. Rev. B **72**, 064427 (2005); S. O. Demokritov, B. Hillrbrands, and A. N. Slavin, Phys. Rep. **348**, 441 (2001).
[7] A. Ercole, A. O. Adeyeye, J. A. C. Bland, and D. G. Hasko, Phys. Rev. B **58**, 345 (1998).
[8] G. Gubbiotti, P. Candeloro, L. Businaro, E. Di Fabrizio, A. Gerardino, R. Zivieri, M. Conti, and G. Carlotti, J. Appl. Phys. **93**, 7595 (2003).
[9] A. Barman, V. V. Kruglyak, R. J. Hicken, J. M. Rowe, A. Kundrotaite, J. Scott, and M. Rahman, Phys. Rev. B **69**, 174426 (2004).
[10] M. Belov, Z. Liu, R. D. Sydora, and M. R. Freeman, Phys. Rev. B **69**, 094414 (2004).
[11] F. Giesen, J. Podbielski, T. Korn, M. Steiner, A. Van Staa, and D. Grundler, Appl. Phys. Lett. **86**, 112510 (2005).
[12] M. Bailleul, R. Höllinger, and C. Fermon, Phys. Rev. B **73**, 104424 (2006).
[13] T. J. Silva, C. S. Lee, T. M. Crawford, and C. T. Rogers, J. Appl. Phys. **85**, 7849 (1999).
[14] A. A. Tulapurkar, Y. Suzuki, A. Fukushima, H. Kubota, H. Maehara, K. Tsunekawa, D. D. Djayaprawira, N. Watanabe, and S. Yuasa, Nature (London) **438**, 339 (2005).
[15] J. C. Sankey, P. M. Braganca, A. G. F. Garcia, I. N. Krivorotov, R. A. Buhrman, and D. C. Ralph, Phys. Rev. Lett. **96**, 227601 (2006).
[16] H. J. Juretschke, J. Appl. Phys. **31**, 1401 (1960); W. M. Moller and H. J. Juretschke, Phys. Rev. B **2**, 2651 (1970); W. G. Egan and H. Juretschke, J. Appl. Phys. **34**, 1477 (1963).
[17] A. Yamaguchi, H. Miyajima, T. Ono, Y. Suzuki, and S. Yuasa, Appl. Phys. Lett. **90**, 182507 (2007); A. Yamaguchi, H. Miyajima, S. Kasai, and T. Ono, *ibid.* **90**, 212505 (2007); A. Yamaguchi, H. Miyajima, T. Ono, Y. Suzuki, and S. Yuasa, *ibid.* **91**, 132509 (2007).
[18] M. V. Costache, M. Sladkov, C. H. van der Wal, and B. J. van Wees, Appl. Phys. Lett. **89**, 192506 (2006); M. V. Costache, S. M. Watts, M. Sladkov, C. H. van der Wal, and B. J. van Wees, *ibid.* **89**, 232115 (2006); J. Grollier, M. V. Costache, C. H. van der Wal, and J. Van Wees, J. Appl. Phys. **100**, 024316 (2006).
[19] N. Mecking, Y. S. Gui, and C.-M. Hu, Phys. Rev. B **76**, 224430 (2007); Y. S. Gui, N. Mecking, X. Zhou, Gwyn Williams, and C. -M. Hu, Phys. Rev. Lett. **98**, 107602 (2007).
[20] J. C. Slonczewski, J. Magn. Magn. Mater. **159**, L1 (1996).
[21] L. Berger, Phys. Rev. B **54**, 9353 (1996).
[22] C. P. Wen, IEEE Trans. Microwave Theory Tech. **17**, 1087 (1969).
[23] M. Gillick, I. D. Robertson, and J. S. Joshi, IEEE Trans. Microwave Theory Tech. **41**, 129 (1993); **41**, 1606 (1993).
[24] 3D Full wave electromagnetic field simulation, produced by Ansoft Corporation.
[25] E. Schlomann, J. Appl. Phys. **33**, 2825 (1962).
[26] A. Yamaguchi, K. Motoi, H. Miyajima, and Y. Nakatani, arXiv:0710.2172 (unpublished).
[27] G. Tatara and H. Kohno, Phys. Rev. Lett. **92**, 086601 (2004).
[28] M. Bailleul, D. Olligs, and C. Ferman, Phys. Rev. Lett. **91**, 137204 (2003).
[29] *Spin Dynamics in Confined Magnetic Structures*, edited by B. Hillebrands and A. Thiaville (Springer, Berlin, Heidelberg, 2006), Vol. III.
[30] K. Yu. Guslienko, S. O. Demokritov, B. Hillebrands, and A. N. Slavin, Phys. Rev. B **66**, 132402 (2002).
[31] A. Thiaville and Y. Nakatani (private communication).
[32] S. Zhang and Z. Li, Phys. Rev. Lett. **93**, 127204 (2004).
[33] A. Thiaville, Y. Nakatani, J. Miltat, and Y. Suzuki, Europhys. Lett. **69**, 990 (2005).
[34] Y. Tserkovnyak and M. Mecklenburg, Phys. Rev. B **77**, 134407 (2008).
[35] The magnitude of a FMR signal induced by the magnetization dynamics can become comparable for a ferromagnet with a certain degree of roughness. In order to completely eliminate such influence on our analysis, a better designed Py strip is required.
[36] J. Shibata, G. Tatara, and H. Kohno, Phys. Rev. Lett. **94**, 076601 (2005).
[37] Although the measured FMR signals contain minor spin-wave modes, all the signals are analyzed by the in-plane mode with a uniform magnetization distribution to simplify the phenomenological analysis. The perpendicular magnetization dynamics induces the dynamic field distribution and the out-of-phase magnetization dynamics.